

Yrast structure of the two-proton- and three-neutron-hole nucleus ^{203}Hg from the decay of a $53/2^+$ isomer

B. Szpak,¹ K. H. Maier,¹ A. S. Smolkowska,^{1,2,*} B. Fornal,¹ R. Broda,¹ M. P. Carpenter,³ N. Cieplicka,¹ R. V. F. Janssens,³ W. Królas,¹ T. Pawlat,¹ J. Wrzesiński,¹ and S. Zhu³

¹*Niewodniczański Institute of Nuclear Physics PAN, Kraków, Poland*

²*Gdańsk University of Technology, Gdańsk, Poland*

³*Argonne National Laboratory, Argonne, Illinois 60439, USA*

(Received 30 March 2011; published 15 June 2011)

The decay of a new, $53/2^+$, isomer at 8281 keV in ^{203}Hg has been studied by γ coincidence spectroscopy. A half-life of 146(30) ns was measured. In addition, another isomeric, $39/2^+$, level with a half-life of 7.8(1.5) ns was observed. Some elements of the Rydstrom shell-model interaction have been adjusted to reproduce level energies in nuclei with two to four holes in the ^{208}Pb core. With this interaction, the new states in the five-hole nucleus ^{203}Hg are reproduced with an rms error of 105 keV.

DOI: [10.1103/PhysRevC.83.064315](https://doi.org/10.1103/PhysRevC.83.064315)

PACS number(s): 23.20.Lv, 27.80.+w, 21.60.Cs, 23.35.+g

I. INTRODUCTION

The shell model, the fundamental building block for the description of nuclei, has lately found renewed and much increased interest. Refined experimental methods allow one to measure properties of “good” shell-model nuclei far away from stability, for example, around ^{78}Ni and ^{100}Sn . Because of the unusual proton-to-neutron ratio and other properties (such as weaker binding, for example), new phenomena may well be found, but in order to recognize their manifestation the properties associated with the “normal” nuclei have to be known well. The region around doubly magic ^{208}Pb has been studied extensively and offers the most complete and detailed information [1] to test the shell model extensively and to determine the relevant interactions between the nucleons. However, rather little is known about neutron-rich nuclei with $Z < 82$. Recently, isomer spectroscopy of fragmentation reaction products has facilitated the study of the semimagic nuclei ^{205}Au and ^{204}Pt ($N = 126$) [2–4]. The results, when taken together with the study of ^{206}Hg [5], provide the most important elements of the effective interaction between proton holes required for the description of high spin states. Thick target γ -coincidence spectroscopy with deep inelastic reactions [6] has proved very successful in studying high spin states in neutron-rich nuclei. Specifically, high spin states in ^{205}Tl [7] and ^{204}Tl [8] have recently been found and the interaction elements between proton and neutron holes determined as a result. High spin states, often of simple structure, can now be predicted using these interactions for Hg nuclei located further away from ^{208}Pb .

In the present experiment, the validity of these effective interactions is tested further by investigating the structural properties of the ^{203}Hg nucleus up to a state with spin $53/2$, the maximum angular momentum that can be achieved through the alignment of the spin vectors of the five valence holes in the ^{208}Pb core. The new results have been compared with

shell-model calculations carried out with the OXBASH code [9] incorporating the effective two-body matrix elements derived from the data discussed above.

Below ^{208}Pb , high spin states are dominated by two intruder orbitals, the $h_{11/2}$ state for protons and the $i_{13/2}$ orbital for neutrons, giving rise to excited states with a particularly simple structure. This is in contrast to the situation above ^{208}Pb , where three high spin orbitals have to be considered for both protons and neutrons.

In earlier work by the present collaboration, deep inelastic processes occurring during heavy-ion collisions at beam energies 20% above the Coulomb barrier were used to study the yrast structure of hard-to-reach, neutron-rich nuclei in the vicinity of ^{208}Pb . For example, detailed γ -ray coincidence measurements in the system $^{208}\text{Pb} + ^{238}\text{U}$ provided information on yrast and near-yrast excitations in ^{206}Hg , $^{210,211}\text{Pb}$, and ^{211}Bi [5,10,11]. A similar experiment with a ^{48}Ca beam and a ^{208}Pb target was instrumental in delineating the yrast structure of ^{208}Bi [12]. The product yield distribution in the latter reaction indicated that nuclei below ^{208}Pb , including ^{203}Hg , had also been populated with cross sections sufficient to undertake a $\gamma\gamma$ spectroscopic analysis. This conclusion was based on the observation of coincidence events between known γ rays emitted in the isomeric or beta decay of the products of interest. Furthermore, a similar analysis of the $\gamma\gamma$ coincidence data accumulated with yet another projectile-target combination, $^{48}\text{Ca} + ^{238}\text{U}$, showed the ^{203}Hg nucleus (a product associated with a 12 proton and up to 23 neutron multinucleon transfer followed by neutron evaporation) was present in this case as well with surprisingly high yield. As a result, a search for higher-lying yrast states in ^{203}Hg was undertaken using the γ -coincidence data sets from both the $^{48}\text{Ca} + ^{208}\text{Pb}$ and $^{48}\text{Ca} + ^{238}\text{U}$ reactions.

II. EXPERIMENTAL PROCEDURE AND RESULTS

The two experiments used to identify the medium-spin yrast structure of ^{203}Hg were performed at Argonne National Laboratory with a ^{48}Ca beam from the Argonne Tandem

*Present address: FOM-Institute AMOLF, Science Park 113, 1098 XG Amsterdam, The Netherlands.

Linear Accelerator System (ATLAS) and the Gammasphere spectrometer [13] which, at the time, was composed of 101 Compton-suppressed Ge detectors. During the first run, a 305-MeV beam was focused on a 50 mg/cm² isotopically enriched ²⁰⁸Pb target. In the second, the projectile energy was 330 MeV and a 50 mg/cm² ²³⁸U target was used. Coincidence data were collected with a trigger requiring three or more Compton-suppressed γ rays to occur in prompt coincidence with each other; the trigger signal was correlated in time to the first coincident γ ray. Energy and timing information was stored for all Ge detectors that fired within 800 ns of the trigger signal. The beam, coming in bursts with ~ 0.3 ns time width, was pulsed with a 412 ns repetition rate to provide a clean separation between prompt and isomeric decays. A total of 8.1×10^8 and 2.3×10^9 three- and higher-fold events were recorded in the first and second measurement, respectively. Conditions on the time parameters were used to obtain various versions of prompt and delayed $\gamma\gamma$ coincidence matrices and $\gamma\gamma\gamma$ cubes covering γ -ray energy ranges up to ~ 4 MeV. Further details about the experiments and the analysis techniques can be found in Refs. [6,14–16].

The highest ²⁰³Hg yrast excitation established prior to this study is the $13/2^+$ isomeric state at 933 keV with $T_{1/2} = 24(4)$ μ s and a predominant $\pi(s_{1/2}^2)0^+ \nu(p_{1/2}^2)0^+ i_{13/2}$ configuration [17]. It decays via a cascade of two transitions of 342 and 591 keV that feed the $9/2^-$ excitation at 591 keV and the $5/2^-$ ground state, respectively. With this information in mind, a search for the high spin structure of ²⁰³Hg was undertaken, first with the data set from the ⁴⁸Ca + ²⁰⁸Pb reaction. Crucial to this procedure is the high detection sensitivity of the Gammasphere spectrometer [13]. In a first step, a spectrum of γ rays coincident with the beam pulse and associated with the subsequent detection (within 1 μ s) of transitions deexciting the $13/2^+$ isomer, i.e., the 342- and 591-keV lines, was investigated: see Fig. 1(a). A few γ rays observed in this spectrum at 192, 375, 639, 705, and 948 keV are candidates for transitions occurring higher in the level scheme of ²⁰³Hg. By exploiting the prompt coincidence histograms, it was found that these newly found γ rays are all in mutual coincidence. As the 375- and 705-keV transitions have the highest intensity, they can be placed just above the $13/2^+$ isomer.

Additional support for the assignment of the observed sequence to ²⁰³Hg came from the analysis of the cross-coincidence relationships with transitions in reaction partners. In the data obtained with the ²⁰⁸Pb target, the complementary products in binary reactions leading to Hg isotopes are Ti nuclei. However, a given Hg nucleus is in coincidence with several Ti partners because of neutron evaporation from the highly excited fragments after the collision. Figure 1(b) presents the spectrum arising from a double coincidence gate placed on the 375- and 705-keV transitions. This spectrum displays known lines from ⁵⁰Ti [18], ⁵¹Ti [19], and ⁵²Ti [20,21], which are the partners of ²⁰³Hg associated with 3, 2, and 1 neutron evaporation, respectively. Further inspection of the spectrum [Fig. 1(b)] revealed, in addition to the Ti partner lines and the transitions at 192, 639, and 948 keV already seen as preceding the $13/2^+$ isomer, the presence of a series of additional γ rays at 146, 219, 261, 492, 533, 540, 847, 889,

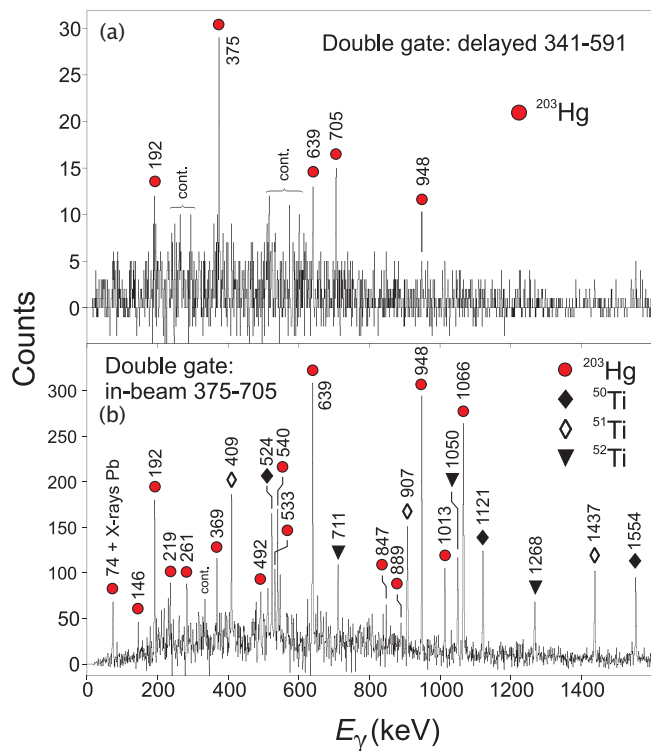


FIG. 1. (Color online) Spectra from the ⁴⁸Ca + ²⁰⁸Pb reaction. (a) Prompt γ rays in double coincidence with the delayed 341- and 591-keV lines from the decay of the 24 μ s, $13/2^+$ isomer in ²⁰³Hg. (b) In-beam γ spectrum double gated by the 375- and 705-keV lines. Transitions in ²⁰³Hg and in the Ti partner nuclei are marked.

1013, and 1066 keV that also belong to ²⁰³Hg. As described below, all these transitions could be used to establish the ²⁰³Hg level scheme given in Fig. 3.

In the course of the analysis, it was noticed that by placing double coincidence gates on the 375- and 705-keV transitions in the off-beam $\gamma\gamma\gamma$ cube from the ⁴⁸Ca + ²³⁸U experiment [Fig. 2(a)], cascades are clearly visible that consist of γ rays that had been assigned to ²⁰³Hg based on the considerations above. Also, additional γ rays appeared in this spectrum at 566, 754, 795, and 1320 keV. It soon became clear that all these transitions belong to cascades deexciting an unknown, high-lying isomer in ²⁰³Hg with a half-life of the order of hundreds of nanoseconds. To locate this metastable state and delineate its deexcitation path, a detailed analysis was performed of spectra resulting from double in-beam and off-beam coincidence gates placed on the newly identified γ rays.

As mentioned above, in the in-beam spectrum gated on γ rays below the $13/2^+$ isomer [Fig. 1(a)], the 375- and 705-keV lines appeared with the highest intensity. Here, a scenario was adopted where the most intense of these at 375 keV (Table I) feeds the $13/2^+$ isomer directly, and the 705 keV γ ray, observed in prompt coincidence with it, originates from a 2013-keV level. Subsequently, by analyzing the intensities of the 192-, 369-, 492-, 540-, 639-, 889-, 948-, 1013-, and 1066-keV lines in the in-beam spectrum doubly gated on the 375- and 705-keV transitions and by exploiting their coincidence relationships as observed in the off-beam

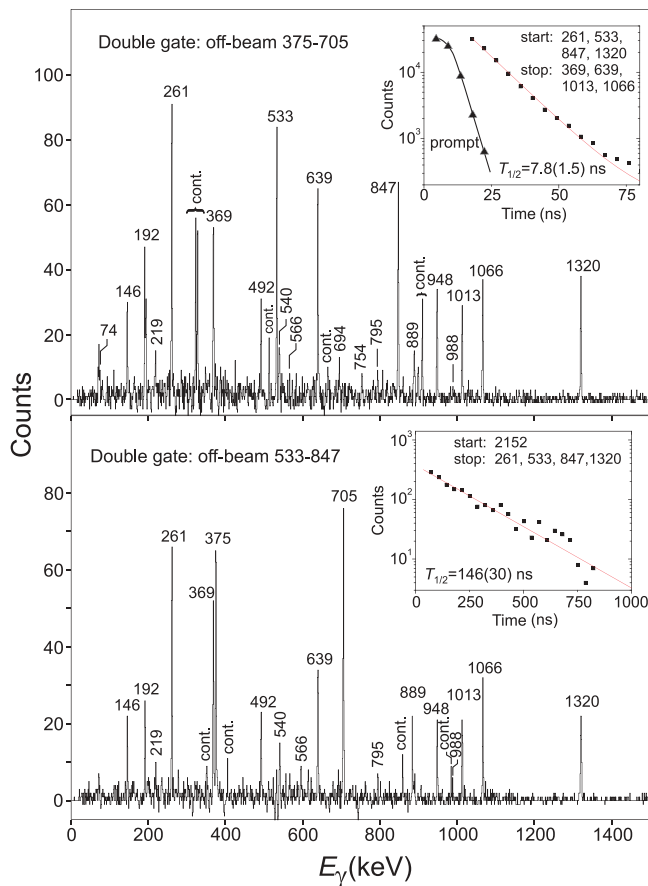


FIG. 2. (Color online) Representative γ spectra from the $^{48}\text{Ca} + ^{238}\text{U}$ reaction. (a) Off-beam spectrum double gated by the 375- and 705-keV lines. The inset shows the summed time distribution between any of the 1320-, 261-, 847-, and 533-keV γ rays used as start lines and any of the 369-, 639-, 1013-, and 1066-keV lines used as stop lines. (b) Off-beam spectrum double gated by the 533- and 847-keV lines. The inset provides the summed time distribution between the 2153-keV γ ray used as a start line and any of the 1320-, 261-, 847-, and 533-keV lines used as a stop line.

$\gamma\gamma\gamma$ cube, levels at 2961, 3079, 3153, 3693, 3792, 4682, 4805, and 5174 keV were established. The other γ rays that appeared as strong lines in the off-beam 375–705 keV coincidence spectrum at 146, 261, 533, 847, and 1320 keV were rather weak in the corresponding in-beam 375–705 keV gate, indicating that they occur rather high in the level scheme. Further support for this scenario came from the analysis of time relationships, which indicated that the 261-, 533-, 847-, and 1320-keV γ rays precede in time (on the scale of tens of nanoseconds) the 146-keV line as well as all other transitions assigned to ^{203}Hg in the present work. As a result of these observations, the 146-keV transition was placed as feeding the 5174-keV level from an isomeric state at 5320 keV. The 261-, 533-, 847-, and 1320-keV γ rays, that had to occur between the two isomers, were found to be in mutual coincidence, but their ordering represented a challenge. However, their in-beam intensities (Table I), when gating on the delayed transitions located below the 5320-keV isomer, clarified the situation and levels at 5852, 6700, 6961, and 8281 keV, where the highest state is an isomer, were

TABLE I. Information on levels and transitions in ^{203}Hg from the present experiment. The energy of the level and of the deexciting γ ray(s) (E_{level} and E_{γ}), the delayed and prompt intensities (I_{delayed} and I_{prompt}), and the ratio of prompt to delayed intensity (Ratio) are presented. See text for details.

E_{level} (keV)	E_{γ} (keV)	I_{delayed}	I_{prompt}	Ratio
1308	374.8(1)	97(7)	100	1.03
2013	705.4(1)	100(10)	97	0.97
2961	948.3(1)	41(2)	39(3)	0.96(8)
3079	1066.3(1)	60(7)	37(3)	0.61(9)
3153	74	40(20)	^a	
	191.6(2)	29(1)	15(1)	0.51(5)
3693	540.2(1)	18(6)	15(2)	0.80(30)
3792	639.2(1)	76(5)	29(3)	0.38(4)
	99	^b	^b	
4587	795.4(1)	10(1)		
4682	889.4(2)	21(3)	5(1)	0.25(6)
	988.4(2)	4(1)		
4805	218.5(2)	11(1)		
	1013.2(1)	55(4)	14(2)	0.26(4)
5174	368.6(2)	54(6)	9(1)	0.16(3)
	492.2(2)	27(2)	4(1)	0.14(3)
5320	145.5(1)	35(10)	4(1)	0.11(4)
5852	532.8(1)	103(19)	6(1)	0.06(1)
6700	847.4(1)	103(17)	4(1)	0.04(1)
6961	261.0(1)	85(10)	3(1)	0.04(1)
	1108	< 3		
7394	694.4(2)	7(1)		
	433(1)	< 4		
7527	565.5(4)	8(2)		
8281	753.9(5)	8(3)		
	887.4(4)	11(4)		
	1320.3(2)	73(8)	1(1)	0.02(1)

^aIntensity cannot be determined because of contaminant Pb X-rays.

^bIntensity cannot be determined because of contaminant U X-rays.

firmly established. The ratio of prompt to delayed intensities (Table I) has to decrease monotonically with excitation energy, independent of branching and detector efficiency. The measured values (Table I) determine clearly the sequence in which some groups of transitions occur as a function of excitation energy. The proposed arrangement of levels in ^{203}Hg received additional support from the observation of weaker transitions that were found only by summing the appropriate coincidence spectra. In this way, a line at 74 keV connecting the 3153- and 3079-keV levels was identified. Also, a cascade of 219- and 795-keV γ rays occurring parallel with the 1013-keV transition and defining an additional level at 4587 keV was established. The spectrum resulting from summing the off-beam coincidence spectra gated on pairs of transitions occurring below the 6700-keV state revealed a 566–754 keV cascade of γ rays parallel to the 1320-keV transition as well as another 887–694 keV cascade from the 8281-keV isomer to the 6700-keV state. Assuming that the 754- and 887-keV transitions originate from the isomer, two new levels at 7527 and 7394 keV are thus established. The presence of a weak 433-keV connection between the 7394- and 6961-keV levels supports these placements. A weak 1108-keV

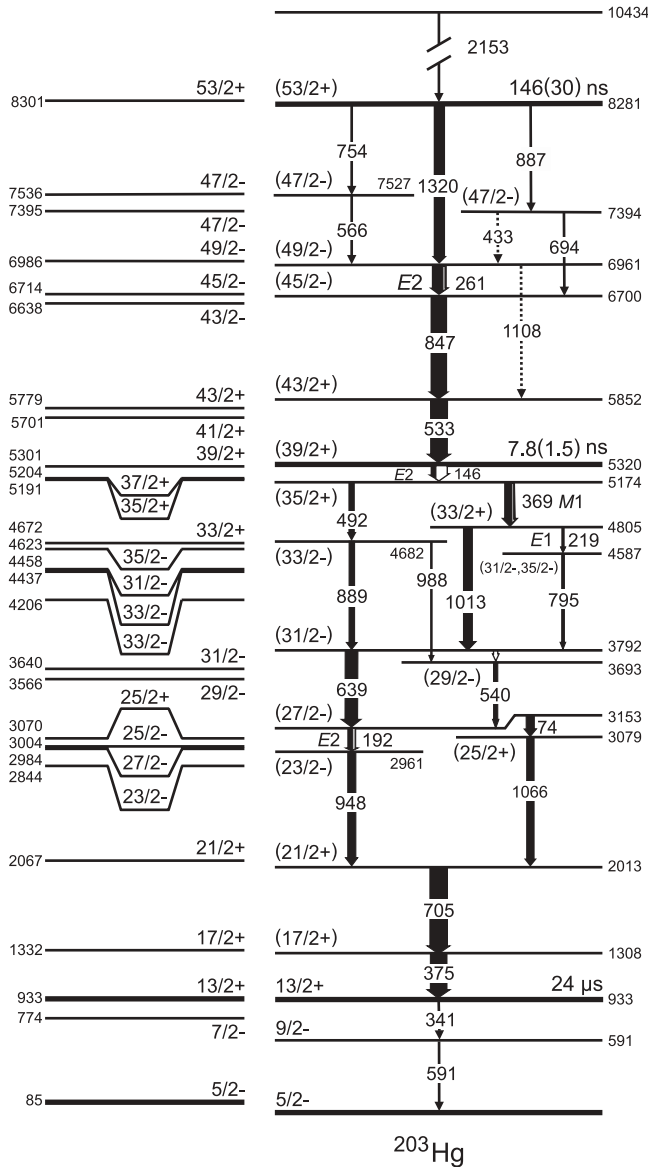


FIG. 3. Proposed decay scheme for the $53/2^+$ isomer in ^{203}Hg (right) compared with a shell-model calculation (left). The energies are relative to ^{208}Pb , but the experimental ground state of ^{203}Hg is set to zero. Transition intensities are indicated by the width of the arrows.

crossover transition from the 6958- to the 5850-keV state was also found. The information on all γ rays presented in Fig. 3 is summarized in Table I. Furthermore, conversion coefficients for low-energy transitions could be deduced, based on missing γ -ray intensities (Table II).

The measured intensities proved crucial to (i) establish the exact sequence of transitions, (ii) indicate the presence of parallel decay paths, and (iii) determine total conversion coefficients used for multipolarity assignments. The efficiency curve of Gammasphere for the present experiments was checked extensively by evaluating well-known cascades in various nuclei produced in the reaction. Since, for low-energy transitions, absorption in the uranium target plays an important role, the efficiency was determined at 147, 182, and 197 keV

TABLE II. Total conversion coefficients deduced from the missing γ -ray intensities. The second column gives the measured delayed intensity, while the third provides the total intensity as expected from the decay scheme. The next columns give the deduced total conversion coefficient and the theoretical conversion coefficients for $E1$, $E2$, and $M1$ multipolarity. The assigned multipolarity is indicated by bold.

E_γ (keV)	I_γ	I_{total}	a_{total}	$E1$	$M1$	$E2$
74	40	60	< 2.0	0.192	3.439	20.48
146	35	100	1.82(83)	0.163	2.682	1.219
192	29	41	0.42(8)	0.083	1.257	0.458
219	11	10	< 0.1	0.059	0.858	0.287
261	85	93	0.09(16)	0.039	0.528	0.163
369	54	65	0.21(14)	0.017	0.206	0.059
375	97	100	0.03(13)	0.017	0.197	0.056

from γ -ray cascades following beta decay of ^{96}Y [22] and isomer decays in ^{130}Te [23] and ^{120}Sn [24]. These nuclei were produced by fission of the target-like products. On this basis, the efficiency for detecting the 146- and 192-keV transitions was established and the corresponding conversion coefficients were determined. These are critical for spin-parity assignments.

Among the newly identified states, those located at 5320 and 8281 keV are isomers. Their half-lives were determined from the time-difference spectra between γ rays cascading into and transitions decaying from the isomer. The time spectrum for the 5320-keV metastable state, obtained by using the 261-, 533-, 847-, and 1320-keV transitions as preceding the isomer and the 369-, 639-, 1013-, and 1066-keV lines as deexciting it [inset in Fig. 2(a)], yielded an half-life of 7.8(1.5) ns. It is worth noting that the analysis of the prompt-delayed coincidence matrix was checked in order to search for γ rays above the 8281-keV isomer. A 2153-keV line was established in this way. Subsequently, the time-difference spectrum between this 2153-keV line and the 261-, 533-, 847-, and 1320-keV γ rays [inset of Fig. 2(b)] indicated a half-life of 146(30) ns for the 8281-keV metastable state. The spin-parity assignments to the isomeric states, as well as to all other levels located in the present work (Fig. 3), are largely based on a comparison with theory and are discussed following the presentation of the shell-model calculations.

III. SHELL-MODEL CALCULATIONS AND INTERACTION ADJUSTMENTS

Shell-model calculations have been performed with the OXBASH computer code [9] without any restriction on the configuration space extending between ^{132}Sn and ^{208}Pb and including the $g_{7/2}$, $d_{5/2}$, $d_{3/2}$, $s_{1/2}$, and $h_{11/2}$ proton orbitals and the $h_{9/2}$, $f_{7/2}$, $f_{5/2}$, $p_{3/2}$, $p_{1/2}$, and $i_{13/2}$ neutron states. The single-particle energies were taken from the latest experimental excitation energies of the appropriate states in one-hole nuclei, and the 2003 mass evaluation tables [25]. The starting point for the two-body matrix elements was the p - n and p - p interactions of Rystroem *et al.* [26], and the n - n interaction

by McGrory and Kuo [27]. These interactions are based on the realistic interaction of Kuo and Herling [28]. McGrory and Kuo used the “bare interaction” of Ref. [28] plus the “bubble” contribution multiplied by 0.75 for the Pb isotopes, whereas Rydstroem *et al.* [26] adjusted some diagonal matrix elements to reproduce more accurately the level energies in ^{206}Tl and ^{206}Hg known at that time.

This interaction has now been adjusted and complemented by considering revised single-proton energies as well as energies of more recently located states, particularly those of high spin that involve the $h_{11/2}$ proton and $i_{13/2}$ neutron. Table III provides the comparison between the two-body matrix elements (TBMEs) used by Rydstroem *et al.* [26] and those obtained in the present work as discussed below.

Along this line, because the mass of ^{207}Tl has been revised [25], all proton-hole energies have been changed by -9 keV from the values used by Rydstroem *et al.* [26]. As a consequence, the 23 two-body matrix elements that Rydstroem *et al.* [26] had adjusted to fit experimental levels had to be changed by $+9$ keV for Tl and $+18$ keV for Hg nuclei. Furthermore, by varying the most relevant diagonal matrix elements of the interaction, a series of OXBASH calculations was performed for 15 yrast states recently identified in the two-hole nuclei ^{206}Pb [29], ^{206}Tl [30], and ^{206}Hg [5], until the level energies were reproduced. Such an iterative procedure was also carried out for the levels already known to Rydstroem *et al.* [26], determining in total 38 TBMEs. For 19 of these, the changes were below 10 keV after adjusting the proton single-particle energies. The error on the ^{207}Tl mass is 5.5 keV [25] and the proton-proton TBMEs have an additional common error of 20 keV from the uncertainty in the ^{206}Hg ground-state mass [25].

As further adjustments, three p - p matrix elements have been taken from newly located states in ^{204}Pt [4]. Among these is the only nondiagonal element that has been modified. The energy difference between the $19/2^+$ and $15/2^+$ levels in ^{205}Au [2,3] relates the unknown $(\pi h_{11/2}\pi s_{1/2}; 6^-)$ element to the known $(\pi h_{11/2}\pi s_{1/2}; 5^-)$ TBME. The $(\pi h_{11/2}\nu f_{5/2}; 8^+)$ element has been adjusted to fit the $29/2^+$ state in ^{205}Tl [31] rather than the 8^+ state in ^{206}Tl [30], as the latter one is heavily mixed with the $(\pi d_{3/2}\nu i_{13/2}; 8^+)$ state. Concerning the $(\pi h_{11/2}\nu i_{13/2})$ interaction, only the matrix element corresponding to the maximum coupling, 12^- , is known in ^{206}Tl [30]. However, since the $(\pi h_{11/2}\nu i_{13/2}^2; 35/2^-)$ state in ^{205}Tl [31] and the $(\pi h_{11/2}\nu i_{13/2}^3; 22^-)$ excitation in ^{204}Tl [8] also contain the coupling to 11^- and 10^- , the corresponding TBMEs could be deduced. Likewise, the $(\nu i_{13/2}^2; 10^+)$ element can be taken from the stretched $(\nu i_{13/2}^3; 33/2^+)$ level in ^{205}Pb [31]. The adopted $(\nu i_{13/2}\nu i_{13/2}; 12^+)$ element results in the energy of the 12^+ state in ^{206}Pb [30] being too high by 5 keV, but it was chosen on purpose in order to better reproduce the corresponding states in $^{204,205}\text{Pb}$ [31,32], as this is more relevant for ^{203}Hg . The value adopted for the $(\nu f_{5/2}^2; 4^+)$ element gives the 4^+ energy in ^{206}Pb [30] too high by 40 keV. This is the largest discrepancy found in the present work, but it was proposed considering that the $(\nu f_{5/2}^2\nu i_{13/2}; 21/2^+)$ state in

TABLE III. Comparison between diagonal two-body matrix elements (in MeV) from the original Rydstroem interaction [26] and described in the present work. Note that the single nondiagonal matrix element is presented at the bottom.

Matrix element	Spin	Rydstroem <i>et al.</i> [26]	Present work
$\pi d_{5/2}\pi s_{1/2}$	2	-0.033	0.198
$\pi d_{5/2}\pi s_{1/2}$	3	0.275	0.505
$\pi d_{3/2}\pi s_{1/2}$	2	0.360	0.354
$\pi d_{3/2}\pi h_{11/2}$	7	0.047	0.173
$\pi s_{1/2}\pi s_{1/2}$	0	-0.327	-0.301
$\pi s_{1/2}\pi h_{11/2}$	5	0.180	0.202
$\pi s_{1/2}\pi h_{11/2}$	6	0.506	0.615
$\pi h_{11/2}\pi h_{11/2}$	8	0.279	0.300
$\pi h_{11/2}\pi h_{11/2}$	10	0.316	0.400
$\nu f_{7/2}\nu f_{5/2}$	1	-0.042	-0.050
$\nu f_{7/2}\nu f_{5/2}$	6	-0.303	-0.193
$\nu f_{7/2}\nu p_{1/2}$	3	0.030	0.153
$\nu f_{7/2}\nu i_{13/2}$	10	0.240	0.147
$\nu f_{5/2}\nu f_{5/2}$	0	-0.190	-0.160
$\nu f_{5/2}\nu p_{3/2}$	3	0.109	0.101
$\nu f_{5/2}\nu p_{3/2}$	4	-0.060	-0.000
$\nu f_{5/2}\nu p_{1/2}$	2	-0.134	-0.146
$\nu f_{5/2}\nu p_{1/2}$	3	0.134	0.141
$\nu f_{5/2}\nu i_{13/2}$	5	0.040	0.052
$\nu f_{5/2}\nu i_{13/2}$	6	0.109	0.102
$\nu f_{5/2}\nu i_{13/2}$	7	0.025	0.017
$\nu f_{5/2}\nu i_{13/2}$	8	0.134	0.122
$\nu f_{5/2}\nu i_{13/2}$	9	-0.150	-0.153
$\nu p_{3/2}\nu p_{1/2}$	1	0.185	0.175
$\nu p_{3/2}\nu p_{1/2}$	2	-0.037	-0.005
$\nu p_{3/2}\nu i_{13/2}$	5	-0.193	-0.221
$\nu p_{3/2}\nu i_{13/2}$	8	0.137	0.194
$\nu p_{1/2}\nu p_{1/2}$	0	0.025	0.010
$\nu p_{1/2}\nu i_{13/2}$	6	0.131	0.126
$\nu p_{1/2}\nu i_{13/2}$	7	-0.003	-0.005
$\nu i_{13/2}\nu i_{13/2}$	10	0.069	0.061
$\nu i_{13/2}\nu i_{13/2}$	12	0.138	0.136
$\pi d_{3/2}\nu f_{5/2}$	1	-0.452	-0.444
$\pi d_{3/2}\nu f_{5/2}$	4	-0.860	-0.848
$\pi d_{3/2}\nu p_{1/2}$	1	-0.264	-0.226
$\pi d_{3/2}\nu p_{1/2}$	2	-0.694	-0.678
$\pi d_{3/2}\nu i_{13/2}$	5	-0.880	-0.856
$\pi d_{3/2}\nu i_{13/2}$	8	-0.520	-0.448
$\pi s_{1/2}\nu f_{5/2}$	2	-0.550	-0.508
$\pi s_{1/2}\nu f_{5/2}$	3	-0.368	-0.356
$\pi s_{1/2}\nu p_{3/2}$	2	-0.000	-0.986
$\pi s_{1/2}\nu p_{1/2}$	0	-0.820	-0.806
$\pi s_{1/2}\nu p_{1/2}$	1	-0.180	-0.148
$\pi s_{1/2}\nu i_{13/2}$	6	0.300	0.350
$\pi s_{1/2}\nu i_{13/2}$	7	-0.720	-0.704
$\pi h_{11/2}\nu f_{5/2}$	8	-0.460	-0.514
$\pi h_{11/2}\nu p_{1/2}$	5	-0.660	-0.572
$\pi h_{11/2}\nu p_{1/2}$	6	-0.120	-0.032
$\pi h_{11/2}\nu i_{13/2}$	10	-0.148	-0.466
$\pi h_{11/2}\nu i_{13/2}$	11	-0.210	0.118
$\pi h_{11/2}\nu i_{13/2}$	12	-1.720	-1.708
$\pi d_{5/2}\pi h_{11/2}\pi d_{3/2}\pi h_{11/2}$	6	0.062	0.222

^{205}Pb [31], that is more closely related to ^{203}Hg , is fitted better with this value. Finally, the $(\nu p_{3/2}\nu i_{13/2}; 8^-)$ element has been

changed to better fit the $(\nu f_{5/2} \nu p_{3/2} \nu i_{13/2}^2; 16^+)$ level in ^{204}Pb [32].

In general, with these modifications, significantly better agreement between calculated and measured energies of excited states is achieved for Pb, Tl, and Hg nuclei of mass 205 and 204 than was the case with earlier interactions. Also, the excitations in the ^{203}Hg nucleus of interest here are expected to be described better with the new interaction, and this should help in interpreting the experimental level scheme. However, relevant shortcomings of the interaction must be pointed out. First, only a small fraction of the diagonal interaction elements could be adjusted to known states. Secondly, by far too little is known about mixing matrix elements to determine these precisely from experiment. However, the fact that calculations with the original Rydstrom interaction already reproduce well the lower spin states that very often are highly mixed gives some confidence in this part of the interaction.¹

IV. SPIN ASSIGNMENTS

For spin assignments, one fixed point is the isomer at 933 keV known as $13/2^+$, the highest spin measured prior to this work. The other reference is the unique $53/2^+$ isomer, corresponding to the highest spin that can be reached by coupling the angular momenta of the five valence holes. A metastable excitation located at 8281 keV is associated with this maximally aligned state. The 2153-keV line feeding the $53/2^+$ isomer is typical for the collective octupole excitation built on this isomer and is found in many similar cases around ^{208}Pb [33].

Based on other experimental observations, a series of considerations regarding transition multiplicities and state spin-parity assignments can be made. From the measured total conversion coefficients (Table II), an $E2$ multipolarity has been established for the 192-, 146-, and 261-keV transitions, while the γ rays at 74 and 219 keV are of $E1$ and the 99-keV line is of $M1$ character. The measured lifetime of the 5320- and 8281-keV states limits the multiplicities for their γ decay to the $E2$ and $M2/E3$ possibilities, respectively. The prompt character of all other lines indicates $E1$, $M1$, and $E2$ as possible multiplicities. Potentially good but not strictly valid arguments can also be used that, in such a shell-model nucleus, $E1$ transitions occur only if an $M1$ or $E2$ decay is impossible or highly hindered. Also, $M1$ transitions tend to be strongly preferred over $E2$ deexcitations. When making spin-parity assignments, one also has to remember that deep inelastic reactions strongly favor the population of yrast or near-yrast levels and that a monotonic rise of spin with excitation energy is the rule.

Besides these experimental and empirical clues, the assignments have to be based on comparisons with theory. As the level density at the yrast line is low and shell-model calculations are reliable in this region, a unique correspondence between measured and calculated states can be established

¹A table of the interaction elements can be obtained from the authors.

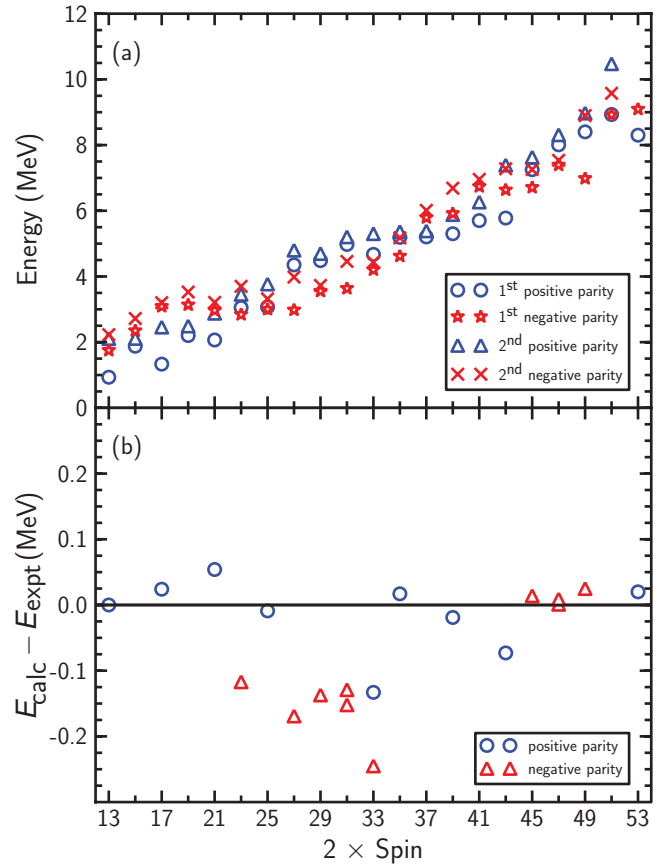


FIG. 4. (Color online) (a) Energies calculated with the adjusted interaction for the two lowest levels in ^{203}Hg of each spin and parity. (b) Difference between calculated and experimental energies in ^{203}Hg relative to ^{208}Pb as a function of spin.

in most cases. Figure 4(a) provides the two lowest calculated levels of each spin and parity as a function of spin. It gives clear indications of the spins to be expected. For instance, above the $13/2^+$ isomer, the $17/2^+$ and $21/2^+$ levels are distinctively low lying. Around spin $23/2$, the situation is unclear and around $31/2$, negative parity is expected. At higher spins, i.e., for yrast levels between spins $35/2$ and $43/2$, positive parity is again predicted, whereas in the $45/2$ – $49/2$ range the levels should have negative parity, according to the calculations.

Starting from the $53/2^+$ isomeric state that arises from a pure $\pi h_{11/2}^2 \nu i_{13/2}^3$ configuration, the tentative spin-parity assignments are proposed as presented in Fig. 3. Three γ decays from the $53/2^+$ isomer can be accommodated by assuming that they feed two $47/2^-$ states and the $49/2^-$ excitation, with the strongest decay branch going to the latter. From the unique configuration $\pi h_{11/2}^2 \nu i_{13/2}^3$ of the $53/2^+$ isomer, $h_{11/2} \rightarrow d_{5/2}$ and $i_{13/2} \rightarrow f_{7/2}$ $E3$ transitions can proceed owing to about 1% admixtures in the final states. These transitions are fast with $B(E3)$ values of about 25 W.u. Taken together, this gives a branching of the order of 1%, as is observed. The dominating transition to the $49/2^-$ level is estimated to have a partial $E3$ half-life of a few 100 ns. The measured lifetime exhibits a hindrance factor of 600 for an $M2$ transition, in accordance with an expected very high

hindrance because, in this case, one of the high-lying $vh_{9/2}$ or $\pi g_{7/2}$ orbitals has to be admixed in the configuration.

Subsequently, the $E2$ multipolarity of the 261-keV decay from the $49/2^-$ level favors a $45/2^-$ assignment for the 6700-keV level, in agreement with the presence of the 694-keV line from $47/2^-$ state and with the calculations [Fig. 4(a)]. Also, no $47/2$ levels are calculated to lie below the $49/2^-$ state. From the calculations, a 76-keV $M1$ decay from the $45/2^-$ state to the $43/2^-$ level is expected. Since it is not observed, the energy difference might be too small or negative in reality. The measured 847-keV line is explained well as an $E1$ transition to the calculated $43/2^+$ state [Fig. 4(a)]—the calculated levels offer no reasonable alternative. Again, an $M1$ transition from the $43/2^+$ state to the nearly degenerate $41/2^+$ level is not seen; instead the predicted $43/2^+ \rightarrow 39/2^+$ $E2$ transition is observed at 533 keV. The next lower level is isomeric—its decay by a 146-keV $E2$ γ ray and its half-life of $T_{1/2} = 7.8(1.5)$ ns agree rather well with the scenario predicted by the calculations where the $39/2^+$ and $35/2^+$ states lie close to one another. The calculated $37/2^+$ level, just below $39/2^+$ state, would destroy the isomerism. Hence, in reality, it probably lies above this $39/2^+$ level. The measured half-life, corresponding to 7 W.u., is typical for an $E2$ deexcitation. The conversion coefficient of the 146-keV line agrees with the $E2$ multipolarity and excludes an $E1$ decay, whereas an $M1$ possibility lies only just outside of the error. However, an $M1$ transition with this lifetime is highly unlikely.

Proceeding now upward from the $13/2^+$ isomer, the $17/2^+$ and $21/2^+$ states are calculated to be yrast and very near the observed energies. The $15/2^+$, $19/2^+$, and all negative-parity states lie distinctly higher in excitation energy [Fig. 4(a)]. Above the $21/2^+$ level, and up to the $35/2^+$ excitation, the calculated yrast states have negative parity, but for spin values of $23/2$, $25/2$ and $33/2$ positive-parity states are sufficiently close to be considered as well. For spin- $27/2$, one negative-parity state is calculated to be 1 MeV lower than any other. Almost certainly, this corresponds to the 3153-keV level. Its decay by the 192-keV $E2$ transition to the $23/2^-$ state and the 74-keV $E1$ transition meet the expectations. Furthermore, the 3079-keV level has a $25/2^+$ assignment and the 1066-keV line consequently has an $E2$ character. Above the $27/2^-$ excitation, the yrast $29/2^-$ and $31/2^-$ levels are calculated to be at very similar energies. The observed levels at 3693 and 3792 keV match this prediction well. They are connected by the 99-keV $M1$ line. Also, their decays by 639- and 540-keV transitions to the $27/2^-$ level are predicted. Going down now from the $35/2^+$ level, the only calculated positive-parity state that can be populated by the 369-keV $M1$ transition is the $33/2^+$ state, which is assigned to a level at 4805 keV. This 4805-keV state decays by a 219-keV $E1$ transition to a 4587-keV level, which may then have either $35/2^-$ or $31/2^-$ quantum numbers, considering that $35/2^-$ and $31/2^-$ excitations are calculated to lie close to it. Also, the 795-keV transition to the $31/2^-$ state allows for both spin values. The 219-, 795-keV sequence is not clear from experiment. The calculations require a parity change below the $33/2^+$ state and the 219-keV $E1$ transition is placed on top. Finally, the only possibility that is left for the 4682-keV state is $33/2^-$. It might correspond to the second $33/2^-$ level

that is calculated to lie 245 keV lower, giving rise to the largest difference encountered during the comparisons between data and calculations presented here. The first calculated $33/2^-$ state is 476 keV below the experimental energy and this excludes it from consideration, as it would be significantly out of the range of the other differences [Fig. 4(b)].

V. DISCUSSION AND OUTLOOK

As the ^{208}Pb nucleus is considered to be one of the best doubly closed cores, the region surrounding this nucleus is a good testing ground for shell-model calculations. Of particular importance in this context is the comparison of experimental data with calculations in which the effective interaction is derived from the free nucleon-nucleon potential without adjustable parameters. Such comparison may provide information on some basic aspects of the nucleon-nucleon interaction or on the renormalization procedure [34]. It turns out that, while a very good agreement has been obtained between results from the recently developed $V_{\text{low-}k}$ realistic shell-model interaction and data for particle-particle and particle-hole nuclei, the agreement for the hole-hole species is not of the same quality [35]. From this point of view, every new piece of spectroscopic information about the hole-hole nuclei, i.e., about the systems lying southwest of ^{208}Pb , would valuably expand the possibility of checking this new realistic shell-model interaction. The ^{203}Hg nucleus studied in the presented work belongs to this region and thus offers the potential for instructive comparisons.

However, in the present study, it was decided to perform shell-model calculations with the improved version of the empirical RYDSTROM interaction rather than with the new realistic interaction. The reason for this approach is straightforward: most spin-parity assignments to the states in ^{203}Hg rely heavily on comparisons with shell-model calculations and an interaction that provides reliable predictions is required in this case. The RYDSTROM interaction was improved by adjusting some diagonal two-body matrix elements in such a way that these new calculations also reproduce the states in $^{205,204}\text{Pb}$, $^{205,204}\text{Tl}$, ^{206}Hg , ^{205}Au , and ^{204}Pt measured in recent years. Since the changes in two-body matrix elements are purely empirical, one can expect that such a modified interaction should be the most adequate to describe the ^{203}Hg experimental data. Indeed, the correspondence between the newly located states and the calculations utilizing the modified interaction is striking. The ground-state mass and the $53/2^+$ isomer at 8281 keV are calculated only 85 and 20 keV above the experimental values, respectively. Furthermore, the mean square difference between the theoretical and experimental level energies is 105 keV and the average linear deviation is -31 keV, illustrating the suitability of the effective interaction. The main discrepancy occurs for the negative parity states between $27/2$ and $31/2$. In the calculations, the wave functions of these states are quite complex: typically, around 15 configurations are involved with a probability of $> 1\%$ and the largest probability is only between 10% and 30%. The deviation between experiment and theory may reflect shortcomings arising from the lack of knowledge about the nondiagonal matrix elements. Another noteworthy systematic feature is that $M1$ transitions predicted by the calculations

to occur between $45/2$ and $43/2$ as well as between the analogous pairs $43/2^+$, $41/2^+$ and $39/2^+$, $37/2^+$ have not been observed experimentally. This nonobservation may suggest an opposite ordering of the state energies within the mentioned pairs of excitations. Here, as well, a possible explanation may be related to the high complexity of the wave functions involved, in which case the state energy would be sensitive to the nondiagonal matrix elements that are not known experimentally.

Summarizing, the shell-model calculations with a new empirical effective interaction, proposed here on the basis of adjustments of some diagonal matrix elements to reproduce the excitation energy of levels that were recently located in nuclei near the doubly closed core ^{208}Pb , provide a surprisingly good agreement with the measured yrast and near-yrast structure of the two-proton- three-neutron-hole nucleus ^{203}Hg . It is hoped

that this new experimental information will serve as a reference for a realistic hole-hole interaction that can be derived from the free nucleon-nucleon interaction within modern theoretical approaches. This represents an important step to be undertaken before reliable predictions can be made for more exotic nuclear species.

ACKNOWLEDGMENTS

This work is supported by the Polish Ministry of Science and Higher Education under Contract No. N-N202-263238 and by the US Department of Energy, Office of Nuclear Physics, under Contract No. DE-AC02-06CH11357. The authors thank the ATLAS operating staff for the efficient running of the accelerators and John Greene for preparing the targets used in the measurement.

-
- [1] K. H. Maier *et al.*, *Phys. Rev. C* **76**, 064304 (2007).
 - [2] Zs. Podolyak *et al.*, *Phys. Lett. B* **672**, 116 (2009).
 - [3] Zs. Podolyak *et al.*, *Eur. Phys. J. A* **42**, 489 (2009).
 - [4] S. J. Steer *et al.*, *Phys. Rev. C* **78**, 061302(R) (2008).
 - [5] B. Fornal *et al.*, *Phys. Rev. Lett.* **87**, 212501 (2001).
 - [6] R. Broda, *J. Phys. G* **32**, R151 (2006).
 - [7] J. Wrzesiński *et al.*, *Eur. Phys. J. A* **20**, 57 (2004).
 - [8] R. Broda *et al.* (in preparation).
 - [9] B. A. Brown, A. Etchegoyen, N. S. Godwin, W. D. M. Rae, W. A. Richter, W. E. Ormand, E. K. Warburton, J. S. Winfield, L. Zhao, and C. H. Zimmerman, MSU-NSCL Report No. 1289 (unpublished).
 - [10] G. Lane *et al.*, *Nucl. Phys. A* **682**, 71 (2001).
 - [11] G. Lane *et al.*, *Phys. Lett. B* **606**, 34 (2005).
 - [12] B. Fornal *et al.*, *Phys. Rev. C* **67**, 034318 (2003).
 - [13] I. Lee, *Nucl. Phys. A* **520**, 641c (1990).
 - [14] R. V. F. Janssens *et al.*, *Phys. Lett. B* **546**, 55 (2002).
 - [15] B. Fornal *et al.*, *Phys. Rev. C* **70**, 064304 (2004).
 - [16] B. Fornal *et al.*, *Acta. Phys. Pol. B* **26**, 357 (1995).
 - [17] P. Zeyen, K. Euler, V. Grafen, C. Günther, M. Marten-Tölle, P. Schüler and R. Tolle, *Z. Phys. A* **325**, 451 (1986).
 - [18] Z. Elekes, J. Timar, and B. Singh, *Nucl. Data Sheets* **112**, 1 (2011).
 - [19] H. Xiaolong, *Nucl. Data Sheets* **107**, 2131 (2006).
 - [20] H. Junde, H. Su, and M. Chunhui, *Nucl. Data Sheets* **108**, 773 (2007).
 - [21] S. Zhu *et al.*, *Phys. Rev. C* **80**, 024318 (2009).
 - [22] D. Abriola and A. A. Sonzogni, *Nucl. Data Sheets* **109**, 2501 (2008).
 - [23] B. Singh, *Nucl. Data Sheets* **93**, 33 (2001).
 - [24] K. Kitao, Y. Tendow, and A. Hashizume, *Nucl. Data Sheets* **96**, 241 (2002).
 - [25] G. Audi, A. H. Wapstra, and C. Thibault, *Nucl. Phys. A* **729**, 337 (2003).
 - [26] L. Rydström, J. Blomqvist, R. J. Liotta, and C. Pomar, *Nucl. Phys. A* **512**, 217 (1990).
 - [27] J. B. McGrory and T. T. S. Kuo, *Nucl. Phys. A* **247**, 283 (1975).
 - [28] T. T. S. Kuo and G. Herling, U.S. Naval Research Laboratory Report No. 2258, 1971 (unpublished); G. Herling and T. T. S. Kuo, *Nucl. Phys. A* **181**, 113 (1972).
 - [29] J. Enders *et al.*, *Nucl. Phys. A* **724**, 243 (2003).
 - [30] F. G. Kondev, *Nucl. Data Sheets* **109**, 1527 (2008).
 - [31] F. G. Kondev, *Nucl. Data Sheets* **101**, 521 (2004).
 - [32] C. J. Chiara and F. G. Kondev, *Nucl. Data Sheets* **111**, 141 (2010).
 - [33] M. Rejmund *et al.*, *Eur. Phys. J. A* **8**, 161 (2000).
 - [34] D. J. Dean *et al.*, *Prog. Part. Nucl. Phys.* **53**, 419 (2004).
 - [35] A. Covello and A. Gargano, *J. Phys. G: Nucl. Part. Phys.* **37**, 064044 (2010).